# DIVERTOR NEUTRAL PRESSURE ENHANCEMENT WITH A BAFFLE IN DIII-D

C.C. KLEPPER[1], J.T. HOGAN[1], D.N. HILL[2], R. MAINGI[3], L.W. OWEN[1], D.A. BUCHENAUER[4], M. Ali MAHDAVI, M.J. SCHAFFER
General Atomics,
San Diego, California,
United States of America

ABSTRACT. The open divertor in DIII-D has been modified by the installation of a baffled plenum with a narrow entrance aperture. Neutral particle pressures in the range of 2–20 mtorr have been measured in this new plenum during experiments in L and H mode plasmas in which the neutral beam power was varied and the divertor target location was scanned with respect to the entrance aperture. These pressures exceed the predicted minimum required to provide adequate particle exhaust for controlling the density in H mode discharges when pumping experiments are conducted in the future. The pressure measurements presented here, which were carried out in the absence of a pump, were modelled with the aid of two transport codes: an edge plasma code and a neutrals code. It was found in this modelling process that the divertor flux amplification factor required to explain the measured pressures is of the order of 30 to 40, much higher than the factors used in the modelling of data in the absence of the baffle. This higher flux amplification factor results from increased recycling at the divertor owing to the presence of the baffle.

## 1. INTRODUCTION

In this paper we present data showing how the installation of a baffle plate near the outer divertor target in the DIII-D tokamak has increased the neutral pressure near the target by more than an order of magnitude for H mode plasmas heated by neutral beam injection (NBI). These high pressures (of the order of 10 mtorr) will facilitate particle removal and thus should help obtain density control in H mode discharges, following the planned installation of a cryopump in the baffle chamber. Figure 1 shows the cross-section of DIII-D with the toroidally continuous baffle plate in place; a typical plasma cross-section for a lower single null configuration is also shown, as is the planned location of the cryopump [1]. This divertor baffle differs from a closed configuration (as in ASDEX [2]), in which the entire divertor region is enclosed by a baffle, and its design is optimized for neutral pressure buildup,

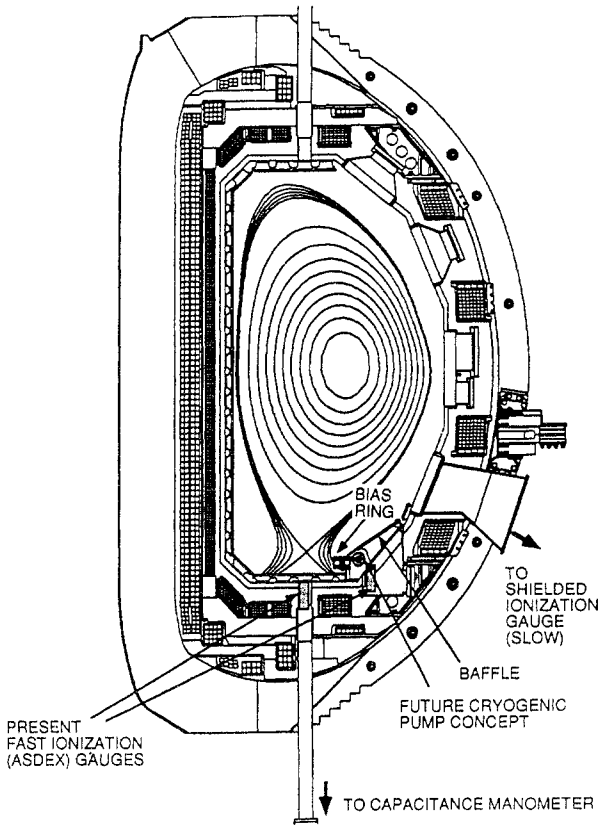


*FIG. 1. A lower single null divertor configuration in DIII-D, with the outer divertor intercept near the bias ring, which forms the throat of the baffle region. Also shown are the locations of the fast ionization gauges.*

[1] *Permanent affiliation:* Oak Ridge National Laboratory, Oak Ridge, Tennessee, United States of America.
[2] *Permanent affiliation:* Lawrence Livermore National Laboratory, Livermore, California, United States of America.
[3] *Permanent affiliation:* North Carolina State University, Raleigh, North Carolina, United States of America.
[4] *Permanent affiliation:* Sandia National Laboratories, Livermore, California, United States of America.

as we discuss below. The installation of the divertor baffle is part of the Collaborative Advanced Divertor Program [3] on DIII-D.

The baffle forms a pumping plenum, which is closely coupled to the divertor plasma when the outer divertor intercept (ODI) is located near the baffle entrance. The 3 cm high entrance channel (or throat) is toroidally continuous and is defined on the bottom by the divertor tiles and on the top by the insulated face of a bias ring. The top of the ring is covered with graphite tiles like the rest of the divertor targets and it can be electrically biased relative to the rest of the vacuum vessel. Our experiments were carried out with the ring at ground potential; details of biasing experiments may be found in Ref. [4].

The pressure under the baffle is a sensitive function of the total ion flux to the divertor plate, and to the location of the ODI relative to the entrance. We define the *gap* to be the perpendicular distance from the separatrix flux surface to the edge of the bias ring, as in Fig. 2. A configuration with a positive gap is shown; a negative gap would correspond to the ODI hitting the vertical face of the bias ring.

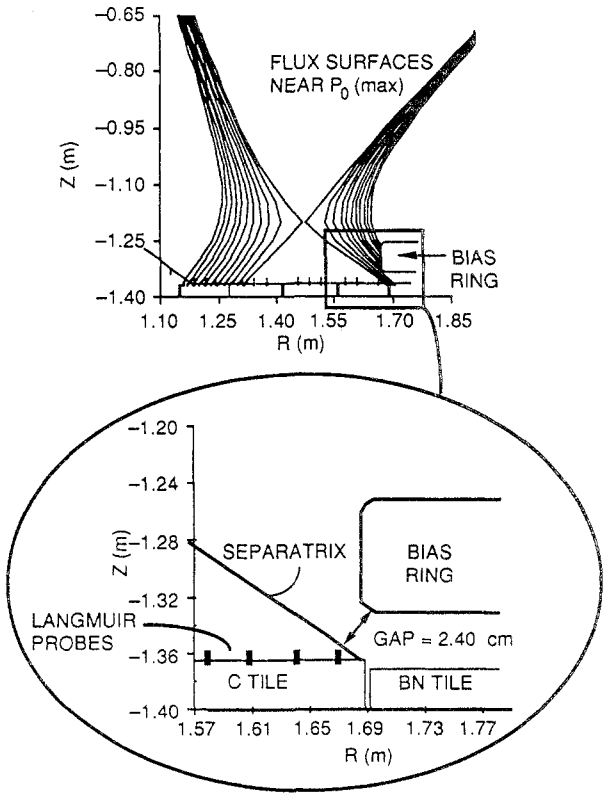


*FIG. 2. Position of the separatrix near the bias ring at the time of maximum neutral pressure in the baffle region for the 7.5 MW case.*

The pressure under the baffle is determined by the particle flux balance in the throat. Without pumping, and neglecting plasma–neutral interactions in the throat, this balance can be expressed in the form $\Gamma_{in} = C_{mol} \times p$, where $C_{mol}$ is the molecular gas conductance back out of the throat and p the pressure under the baffle. The flux into the throat results from the neutral recycling that occurs where the scrape-off layer (SOL) plasma strikes the divertor targets. Thus,

$$\Gamma_{in} = r \times f_1 \times f_2 \times \Gamma_{div}$$

where $\Gamma_{div}$ is the total ion flux to the outer divertor target, r is the recycling coefficient at the target plate, and $f_1$ and $f_2$ are, correspondingly, the fractions of the recycled neutrals that head toward the throat and that pass through the divertor plasma without reionization. The product $f_1 \times f_2$ is of the order of 0.1 and represents the collection efficiency of the entrance throat. This order of magnitude estimate can be made by taking into consideration the geometric relation between the distribution of recycled neutrals at the ODI and at the entrance of the throat, and also the ionization path length for neutrals in the divertor plasma. More detailed calculations require the use of a neutral particle transport code, such as DEGAS [5], which is used in this study.

It is the sensitivity of the collection efficiency to the gap that is primarily responsible for the strong dependence of the pressure under the baffle on the gap. On the one hand, as the gap becomes very large, the entrance of the throat subtends a smaller angle for the collection of particles originating from the ODI and neutrals must traverse more plasma before entering the throat. On the other hand, as the gap becomes very small, a large part of the particle flux density profile at the divertor is truncated by the bias ring. Qualitatively, we expect that the truncation of the profile by the entrance aperture will cause a reduction in the entrant neutral particle flux when the distance from separatrix to aperture becomes too small. Therefore, we expect a strong dependence of the neutral pressure on the gap. The effect of this truncation on the total flux entering the plenum depends strongly on the actual profile of the flux density. Therefore, the dependence of the pressure on the gap size depends strongly on the actual profile of the SOL plasma near the throat. The experiments discussed in this paper have demonstrated this effect by means of radial sweeps of the ODI across the entrance of the baffled region.

As already indicated, the main purpose of the divertor baffle is to facilitate particle exhaust with the future installation of a cryopump in the baffled region. In order to obtain H mode density control, the pumping

system must at least remove gas at a rate greater than or equal to the fuelling rate from neutral beam heating, which is about 20 torr·L·s$^{-1}$ with 20 MW of beam heating. With the present design we expect to achieve a pumping speed of 50 000 L/s, so that plenum pressures near 1 mtorr will be required to obtain an exhaust rate of 20 torr·L·s$^{-1}$ [6]. Calculations with the DEGAS neutrals code were used to optimize the design height of the aperture and the width of the bias ring. Early DEGAS calculations [6] suggested that, with a neutral beam power of $P_{inj} \simeq 7$ MW, a maximum pressure of $p_{baffle}^{max} \sim 1$ mtorr could be expected for the DIII-D baffle geometry without pumping, and of $p_{baffle}^{max} \simeq 0.5$ mtorr with pumping.

Initial experiments at low auxiliary power with the ODI placed near the throat of the baffle region readily demonstrated that pressures were in excess of 3 mtorr [7]. In addition, electrical biasing of the ring was shown to have a large effect on this pressure. Compared with a large database of shots before the installation of the baffle,
such pressures are about an order of magnitude higher than the highest pressures measured near the outer leg of the separatrix without a baffle.

With the intention to optimize this pressure buildup further, the experiments presented here were designed for a systematic study of the dependence of the pressure on both the injected power and the magnetic geometry. The plasma for these experiments was shaped in a lower single null divertor (SND) configuration with plasma current $I_p$ = 1–1.25 MA and chord averaged electron densities of approximately $3.5 \times 10^{19}$ m$^{-3}$. This study includes a power scaling in the H mode with 4.5 to 14 MW of injected neutral beam power. For comparison, we have also studied the low power L mode and ohmically heated discharges. All discharges were at a magnetic field of $B_T$ = 2.1 T. Deuterium was used both as the working gas and in the neutral beams. The plenum neutral pressure ranged from about 2 to 16 mtorr, proportional to the neutral beam injection power. Comparison with modelling will show that recycling played a large role in this increase of the pressure with injected power.

The paper is arranged as follows. In Section 2, we describe the diagnostics used in the pressure measurement, other supporting diagnostics, and the set-up of the plasma discharge. In Section 3, we describe the experimental results. In Section 4, we discuss the analysis and interpretation of the data, which includes modelling using a combination of the SOL plasma code with the DEGAS neutrals code. Conclusions are presented in Section 5.

## 2. EXPERIMENTAL TECHNIQUE

The pressure under the baffle was measured with a fast ionization gauge. This type of gauge, originally developed at the Max-Planck-Institut für Plasmaphysik, Garching, employs the magnetic field of the tokamak in its operation [8, 9]. As such, it can be located inside the vacuum vessel and is capable of a fast time response (<5 ms). The time response is limited by the conductance of a housing built around the gauge to prevent plasma ions and energetic neutrals from directly reaching the collector. The emission current of these gauges is modulated at approximately 10 kHz for both background subtraction and noise reduction. In addition to the primary gauge located under the divertor baffle, a second gauge, located at a port on the tiled floor of the machine and approximately under the X point in an SND discharge (Fig. 1), was used to measure the pressure in the private flux region.

Before the experiment, these gauges were calibrated over a large range of pressures (from about 0.2 to 20 mtorr). The calibration was done against a capacitance manometer with the machine backfilled with deuterium. Shots with toroidal field only (no plasma) and with data acquisition were used in this calibration. Gas puffing during the toroidal field flattop was used to obtain three pressure levels per shot. This calibration was of particular importance at many values of the pressure in the high pressure range (above 5 mtorr) because of a significant non-linearity in the dependence of the ion current on the pressure [9].

The objective of the experiments was to determine the maximum pressure that could be achieved under the baffle for different plasma conditions. The maximum pressure was expected to occur at some optimal position of the ODI with respect to the entrance of the baffled region. Because of the concern that the optimal position for pressure buildup under the baffle might vary as a function of $P_{inj}$ and $I_p$, the position of the ODI was swept across the aperture of the baffled region. The sweep rate was slow enough to allow equilibration of the pressure under the baffle at each position. The smallest resolvable displacement was assumed to be 0.5 cm. Each sweep was made in 1400 ms and covered approximately 5 cm in radial extent. This allows for approximately 140 ms of equilibration time.

The total volume under the divertor baffle is approximately $V_{baffle} = 1.8 \times 10^6$ cm$^3$, and the conductance to that region from the main vessel is estimated to be $C_{mol} = 5 \times 10^7$ cm$^3$/s. Therefore, the time to fill the closed divertor region, $\tau_{baffle} = V_{baffle}/C_{mol}$, is about 36 ms. As a result, these position scans covered a period

much longer than the filling time of the plenum volume. They were designed in this way in order to ensure that the recycling at the strike point would also equilibrate, because this is an important parameter in determining the baffle pressure. (We note that the global recycling, which involves all of the tokamak walls, typically requires several seconds. Here we are concerned only with recycling equilibration at the ODI.)

For the purpose of economy in the number of shots, the ODI was swept through twice during each shot — first outward, then inward. With two sweeps, it was possible to obtain two experimental points per shot, at different beam powers or plasma currents. The second (inward) sweep was somewhat faster than the first (averaging about 7.5 cm/s compared with 6.5 cm/s), to cover a larger range. This was done to allow the ODI to pass through the region of the machine floor, where some of the divertor tile Langmuir probes are located.

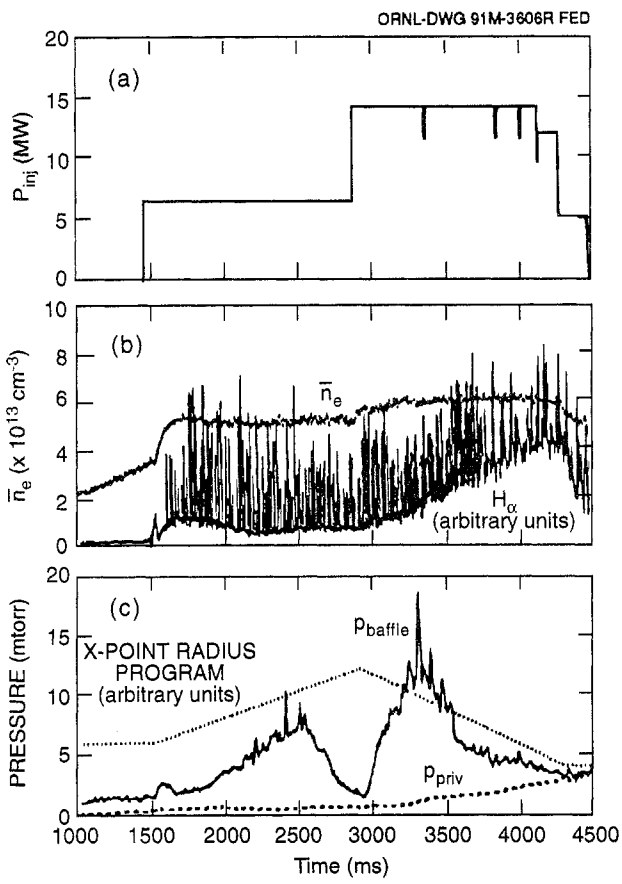


*FIG. 3. Some traces for a typical shot from this experiment, showing (a) the neutral beam injected power, (b) the line averaged electron density with the $H_\alpha$ signal, which shows the ELMs, and (c) the baffle and private flux region neutral pressures together with the position control signal for the X point radius program.*

The outward and inward sweeps were compared under similar conditions.

Figure 3 shows some signal traces for a typical shot (70902). In this shot, the beam power doubles as the number of NBI sources is increased from three to six. In addition to $P_{inj}$ and the pressure under the baffle, the chord averaged electron density, which remains nearly fixed, and the $H_\alpha$ photodiode signal, which shows the edge localized modes (ELMs) during the H mode, are shown. The neutral pressure in the private flux region $p_{priv}$ was added to illustrate that the pressure under the baffle is much higher than the background pressure in the vessel.

Throughout the experiment, the plasma parameters were monitored with standard DIII-D diagnostics. In particular, Thomson scattering was used to obtain both electron temperature and electron density profiles. The high spatial resolution at the edge ($\approx 1.3$ cm) was utilized by appropriately positioning the upper separatrix inside the region of high resolution. The multiple pulse nature of this diagnostic (25 ms repetition rate) allows for a resolution compatible with that of the pressure measurements.

The divertor tile Langmuir probes [10] form a radial array of single-tip probes. The locations of some of the outer divertor probes are shown in Fig. 2. The outermost probe tip is about 2 cm radially inward from the inner edge of the bias ring. This is why the inward sweep had to be extended to cover the probes. Only two of the probe tips were scanned by the ODI before the end of the discharge.

Finally, the lower divertor infrared television camera (IRTV) was used to monitor the power flux density at the ODI during the sweep. The camera views from the top of the machine and converts infrared thermal emission to a calculated temperature of the graphite tiles in its field of view. From this, the divertor heat flux can be inferred [11]. For these experiments, however, the region of peak heat flux density can be shadowed by the ring. For this reason, heat flux profiles for the analysis were usually obtained from a later part of the shot, when the ODI was away from the ring and near the tile Langmuir probes.

## 3. EXPERIMENTAL RESULTS

### 3.1. Neutral pressure dependence on NBI power

Figure 4 shows the dependence of the peak value of $p_{baffle}$ on the injected power. The squares denote the Ohmic and L mode cases, and the circles denote the

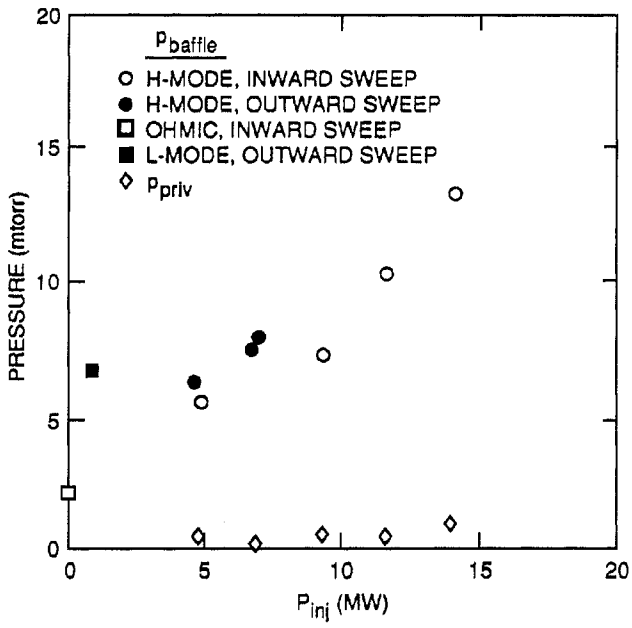


*FIG. 4. Dependence of the baffle pressure on the neutral beam injected power. Pressure in the private flux region is also shown. All data points are for $B_T$ = 2.1 T and $I_p$ = 1.0 MA.*

H mode cases. In the H mode cases, the peak pressure is averaged over the ELMs. Since the direction of the scan may be important, the measurements done during the outward radial scan are depicted with open symbols, while those done during the inward scan are depicted with filled symbols. If we neglect the L mode case, we observe a nearly linear increase of the pressure with power from the Ohmic to the highest power H mode case. The pressure was anticipated to be higher in the L mode case, because the particle confinement time is lower than that of the H mode for the same power. The flux of particles out of the plasma core and into the divertor region and finally into the throat of the baffle region is inversely proportional to the particle confinement time.

Since the pressure under the baffle may also depend on the pressure in the divertor region outside the baffle, it is useful to compare the two. The pressure in the private flux region was measured and is also plotted as a function of the injected power in Fig. 4. We observe that this pressure is about an order of magnitude lower than that under the baffle and does not change significantly with the injected power. From this comparison, we conclude that the background pressure does not contribute to the nearly linear rise of baffle pressure with injected power that we have observed.

### 3.2. Dependence of pressure on magnetic geometry

The position of the divertor strike point with respect to the plenum aperture is an important variable in determining both the flux of particles to the plenum and the interaction of the plasma with the baffle structure. The geometry for the conditions of maximum pressure was determined with the EFITD magnetic fitting code [12, 13]. The code produces an optimal least squares fit to the magnetic probe data on DIII-D. For these

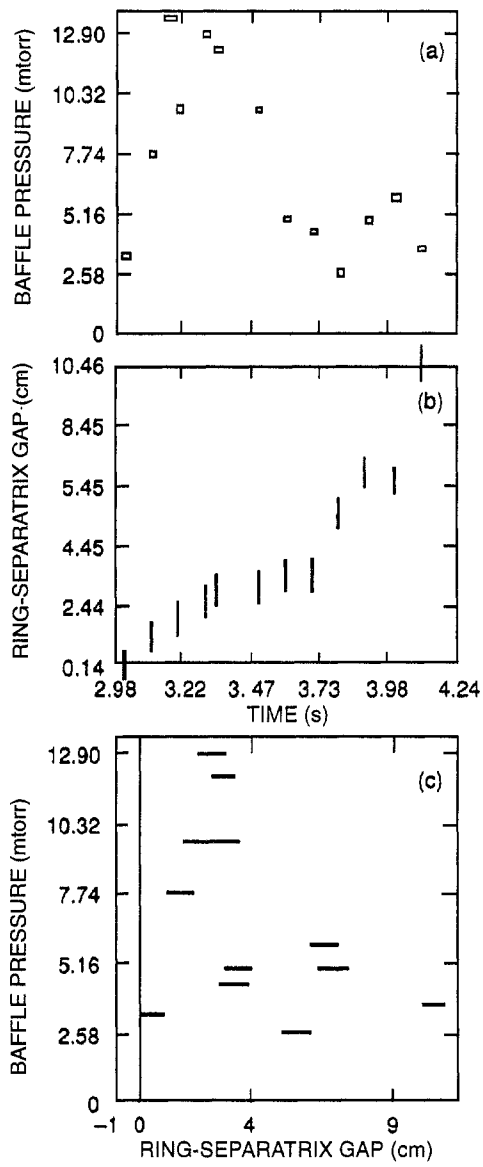


*FIG. 5. Procedure by which the dependence of the pressure on the separatrix-ring gap is determined. The raw data of pressure versus time (a) and the magnetics code results of gap versus time (b) are used together to obtain pressure as a function of gap (c).*

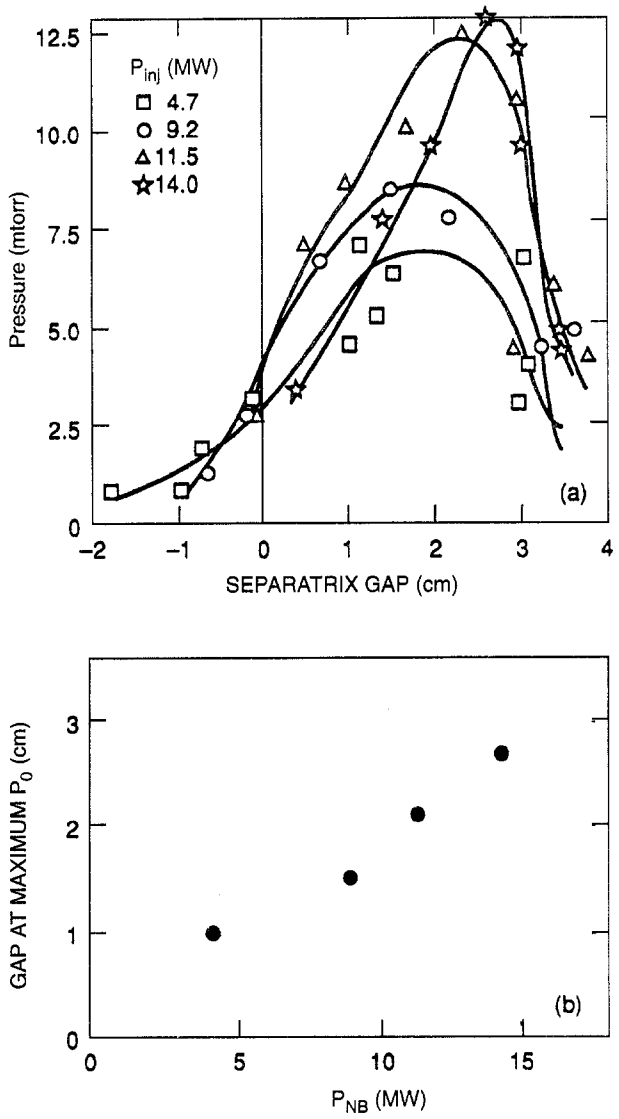


*FIG. 6. (a) Dependence of the neutral pressure on geometry for the power scan series. (b) Optimal gap as a function of injected power.*

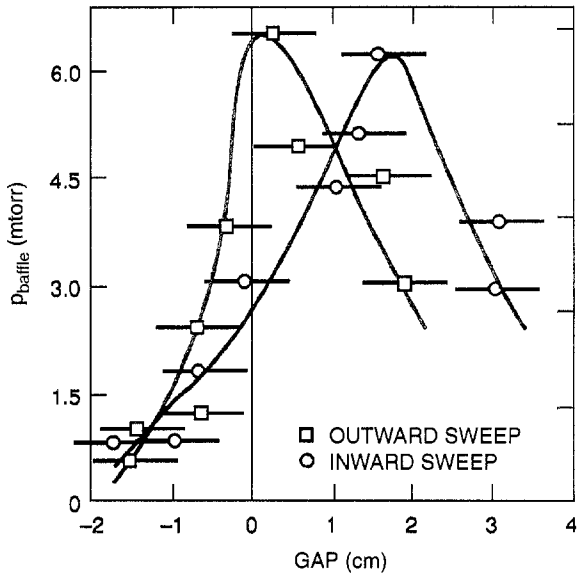


*FIG. 7. Neutral pressure dependence on gap for two discharges with nearly equal injected power but different sweep directions.*

experiments, the determination of the magnetic geometry in the region near the floor of the vessel requires the inclusion of current density profiles with edge currents flowing in the SOL. The separatrix position near the lower floor can be determined only to within about 1 cm with the existing magnetic diagnostics on DIII-D. As seen in Fig. 2, the separatrix at a time near that of maximum pressure for $P_{inj} \simeq 7.5$ MW has a clearance of about 2.4 cm with the bevelled edge of the bias ring. As can be seen, the optimum position is relatively close to the gap between the graphite and boron nitride tiles. An initial concern, after the ODI sweeping experiment, was that the observed high neutral pressure might result, to some extent, from the conditioning of the region near this gap. However, when we carried out a second experiment, many more tokamak discharges later, in which a few similar shots were made with a fixed ODI location near the ring, we obtained reproducible high neutral pressures for 2 to 2.5 s and observed no deterioration of the pressure from shot to shot. This indicates that the graphite tile near the optimal position was near saturation.

Figure 5 illustrates the procedure for determining the dependence of pressure on the separatrix–ring gap. Figure 5(a) shows the data for pressure versus time for a high power case during the inward sweep. The results of a series of EFITD fits to the magnetic probe data, providing a calculation of the gap distance as a function of time, are shown in Fig. 5(b). From these data, the dependence of baffle pressure on the gap, as shown in Fig. 5(c), is produced.

This dependence of pressure on geometry varies with power. The results for a power scaling sequence of H mode discharges are shown in Fig. 6. All of the cases were taken during the inward sweep of the separatrix and show a tendency for an increase in the gap at which the maximum neutral pressure occurs with increasing power.

We also examined the influence of the direction of the plasma sweep on the variation of the neutral pressure with gap. Figure 7 shows the dependence of pressure on the separation distance for two cases, the first with an

outward sweep and the second with an inward sweep, at nearly the same power. As seen in this example, the outward sweeps have consistently smaller optimal gaps than the inward sweeps. However, the sensitivity of the pressure to the gap is the same in both cases. The difference in the optimal gap between the two cases may be attributed to the time history of the interaction between the plasma and the wall away from the ODI. Additional experiments would be required to study this issue systematically.

## 4. ANALYSIS AND DISCUSSION

It is desirable to compare the measured peak pressure under the baffle, and its scaling with gap and power, with what we expect from our models. We first make a simple estimate of the pressure in the plenum for a typical discharge using the measured ion flux to the divertor in order to see if the measurements are reasonable. Then we proceed with more careful modelling using the DEGAS and B2 codes, along with Thomson scattering data ($n_e$, $T_e$ profiles near the midplane) to define the boundary conditions.

### 4.1. Estimate of baffle pressure based on divertor particle flux

The measured ion saturation flux to the divertor target at the ODI, $j_{sat}$, can be used to compute a gross estimate of the ion flux into the plenum. The relationship between baffle pressure, $p_{baffle}$, and incident particle flux, $\Gamma_{in}$, into the baffled plenum is given by

$$V \frac{dp_{baffle}}{dt} = \Gamma_{in}(t) + p(t)C_{mol}$$

where $C_{mol}$ is the molecular conductance of the throat for deuterium and V is the baffle region volume. Evaluated at the time of peak pressure, this equation yields the relationship between peak pressure and flux into the baffle:

$$p_{baffle}^{max} = \Gamma_{baffle}/C_{mol}$$

An estimate of $\Gamma_{baffle}$ can be made from the $j_{sat}$ data:

$$\Gamma_{baffle} = 0.1 \times \frac{j_{sat,peak} \times \lambda_\Gamma \times 2\pi R_{THROAT}}{e \times (7 \times 10^{19})}$$

(with $j_{sat}$ in A/cm$^2$), where the numerical factor in the denominator converts $\Gamma$ into units of torr·L·s$^{-1}$, the electron charge $e = 1.6022 \times 10^{-19}$ C, $\lambda_\Gamma \simeq 2$ cm is the ion flux SOL length and $R_{THROAT} \simeq 170$ cm. The factor 0.1 is the estimate of the particle collection efficiency discussed in Section 1.

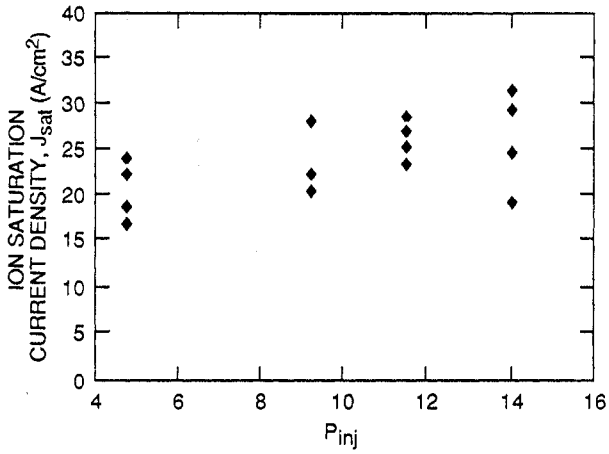


*FIG. 8. Ion saturation current as a function of injected power.*

Spatial particle flux profiles, $j_{sat}(R)$, at the divertor are produced by sweeping the plasma over the Langmuir probes at R = 1.64 m and 1.67 m on the machine floor. Figure 8 shows the ion saturation current density at the times when the outer strike point crossed the probes at R = 1.64 m and R = 1.67 m. As indicated by this figure, the ion saturation current, which is proportional to the ion flux density striking the divertor tiles, does not significantly increase with $P_{inj}$. However, the presence of ELMs causes a large uncertainty in the measurement of the ion saturation current. This is reflected in the large scatter of the data.

In addition to $j_{sat}$, the Langmuir probe data were analysed to give electron temperatures and densities at the ODI. Figures 9(a) and 9(b) show the electron temperatures and densities, respectively, from the Langmuir probes, as a function of the injected power. In contrast to L mode discharges, where most past studies of divertor plasma parameters have been carried out [14], in the H mode the probes are perturbed by the ELMs. During an ELM, $j_{sat}$ rises very sharply and can then fall and remain very low for many milliseconds afterwards. Therefore, even with the analysis made between ELM events, as was done here, the ELMs still affect the results and cause the large scatter seen in the data of Fig. 9. The data are still of interest in ensuring that the plasma parameters resulting from the edge plasma model, to be discussed below, are within the range of the experimental data scatter.

For shot 70902 at 14 MW of NBI power, where the baffle pressure was measured to be about 13 mtorr,

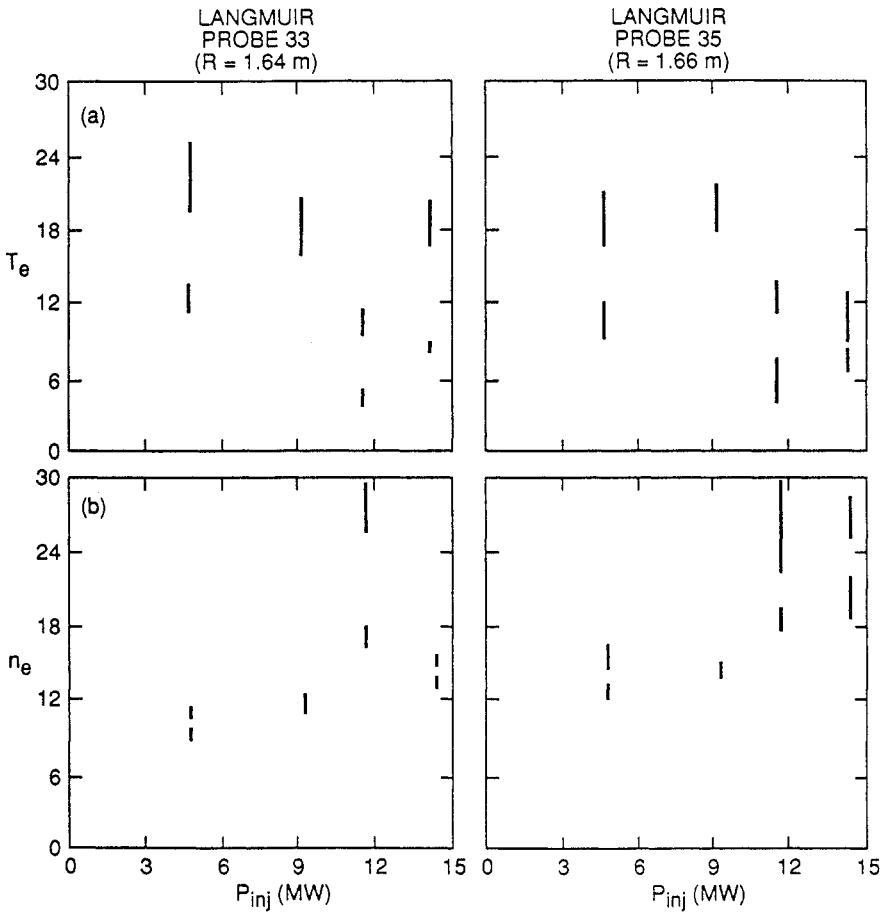


*FIG. 9. (a) Electron temperature and (b) electron density from two tile Langmuir probes, one at 1.64 m and one at 1.67 m, as a function of injected power.*

$j_{sat,peak} \simeq 25$ A/cm$^2$. From the above equation a value of $\Gamma_{baffle} = 428$ torr·L·s$^{-1}$ is obtained. Dividing by the 50 000 L/s estimated value of molecular conductance, a pressure of 8.5 mtorr is obtained. Though the agreement is good, it may be fortuitous. For example, the gas conductance back out of the throat is probably lower than our value, owing to the presence of plasma in the throat [15]. In addition, we have used a value for $j_{sat}$ obtained by the Langmuir probes when the ODI was 3–6 cm from the optimal position where the plenum pressure is at a maximum (Fig. 2). When positioned near the throat, the peak ion flux may be higher since the baffle probably increases the flux amplification factor $\alpha$ [16], defined as the ratio of the particle flux at the plate to the flux across the separatrix out of the core. Previous studies [17] obtained values of $\alpha = 5$–15 for DIII-D, whereas we predict values as high as 20–30 for cases with the plasma near the ring, as shown below.

### 4.2. Modelling of the baffle pressure

Since the pressure under the baffle depends directly on the fraction of recycled neutrals that reach the baffle throat, and this depends on the details of the plasma-neutral interactions near the target plate, we used the DEGAS neutrals transport code to simulate the pressure buildup. The two dimensional (2-D) DEGAS Monte Carlo code [5] computes the trajectories of neutral atoms and molecules released from the target plate given a background divertor/SOL plasma, the wall geometry and the material properties of the nearby surfaces. Appropriate diagnostics in the code provide the total ionization source, neutral density and wall flux needed to interpret our measurements. Because the code requires that plasma parameters ($n_e$, $T_e$) be specified everywhere on the computational grid and we have only limited measurements, we used the

TABLE I. THOMSON SCATTERING VALUES OF $T_e^{sep,midpl}$ AND $n_e^{sep,midpl}$ FOR THREE NBI POWER LEVELS

| Shot | $P_{inj}$ (MW) | $T_e^{sep,midpl}$ (eV) | $n_e^{sep,midpl}$ ($10^{13}$ cm$^{-3}$) | $Q_{IRTV}$, integrated total (MW) |
|---|---|---|---|---|
| 70903, near the ring[a] | 7.5 | 80.0 ± 10.0 | 1.80 ± 0.15 | N/A |
| 70903, away from the ring[b] | 7.5 | 50.0 ± 10.0 | 0.80 ± 0.15 | 0.9 |
| 70902, near the ring[a] | 14 | 200.0 ± 53.1 | 3.44 ± 0.53 | N/A |
| 70902, away from the ring[b] | 14 | 78.12 ± 12.5 | 1.37 ± 0.09 | 1.2 |

**Note:** The error bars represent the uncertainty in determining the actual position of the separatrix from the magnetic probes. The total power to the divertor is also given for the cases in which the IRTV is not shadowed by the bias ring.

[a] Near the ring data are taken when the baffle neutral pressure peaks (~ 3300 ms).

[b] Away from the ring data are taken when the ODI is in view of the IRTV (at t > 3900 ms).

Braams B2 code [18] to generate the plasma consistent with our limited measurements. We have modelled two cases: (a) the 14 MW, 1 MA case (shot 70902) and (b) the 7.5 MW, 1.25 MA case (shot 70903).

### *4.2.1. B2 plasma modelling*

The B2 code [18] solves the plasma transport equations on a 2-D mesh that accurately describes the SOL magnetic geometry. Given a set of transport coefficients ($\chi$, $D_\perp$, $v_{conv}$) and upstream boundary conditions (some combination of density, temperature and/or heat and particle fluxes), the B2 code computes the density and temperature profiles everywhere in the SOL. These can be checked against Thomson scattering data near the midplane and divertor Langmuir probes and IRTV (heat flux) data at the divertor targets away from the baffle throat.

Because we do not have data from the target plates (particle and heat flux, $n_e$ and $T_e$) when the ODI is in the baffle throat under this bias ring, we first determined the appropriate plasma transport coefficients from measurements made when the plasma was well away from the ring. For midplane boundary conditions, we used the Thomson scattering data at 4200 ms, when the ODI is away from the ring. The time resolved electron temperature and density just inside the separatrix, measured near the midplane, are given in Table I for two different values of injected power

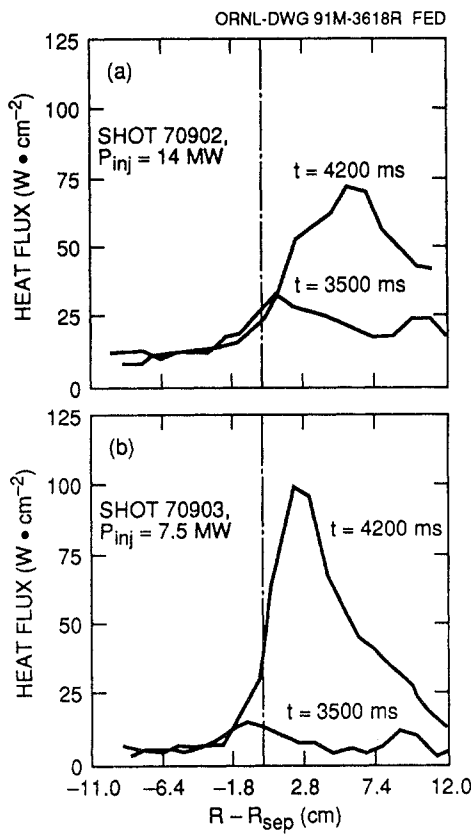


*FIG. 10. The IRTV data at the time of peak pressure, when the peak is shadowed from the camera by the ring, and at 4 s for two cases: (a) 14 MW, 1 MA and (b) 7.5 MW, 1.25 MA.*

(7.5 and 14 MW). Each profile here represents the average of four Thomson measurements taken over a span of 100 ms. Since the edge density profiles are very steep in the H mode, there can be an uncertainty of as much as a factor of two in the midplane values due to uncertainties ($\sim 1$ cm) in the separatrix location. The uncertainties, as computed from the standard deviation of the measurements included in the averages, are also given in Table I.

We found that, given the Thomson scattering values shown in Table I, we could match the measured divertor heat flux profile with the B2 code using the following transport coefficients: $\chi_e = 4$ m$^2$/s, $\chi_i = 0.2$ m$^2$/s (for the electron and ion thermal diffusivities, respectively), D = 4 m$^2$/s (for the particle diffusivity) and v = 40 m/s (for the inward particle pinch). Earlier studies [19] of the DIII-D SOL plasma found similar values for D, $\chi$ and v. The divertor plate recycling coefficient was fixed at 0.99. Figure 10 shows the measured heat flux profiles at the ODI for the two cases modelled ($P_{inj}$ = 14 MW, $I_p$ = 1.00 MA, and $P_{inj}$ = 7.5 MW, $I_p$ = 1.25 MA). An example of a fit to the heat flux profile with model B2 is shown in Fig. 11 (for the 7.5 MW case). The bars represent the model results. The widths of the bars represent the experimental uncertainty in relative flux surface position. Table II summarizes the input and output parameters used in code B2. In addition, we note that good agreement was obtained between modelled peak divertor electron temperatures and those measured with the divertor Langmuir probes (Fig. 9).

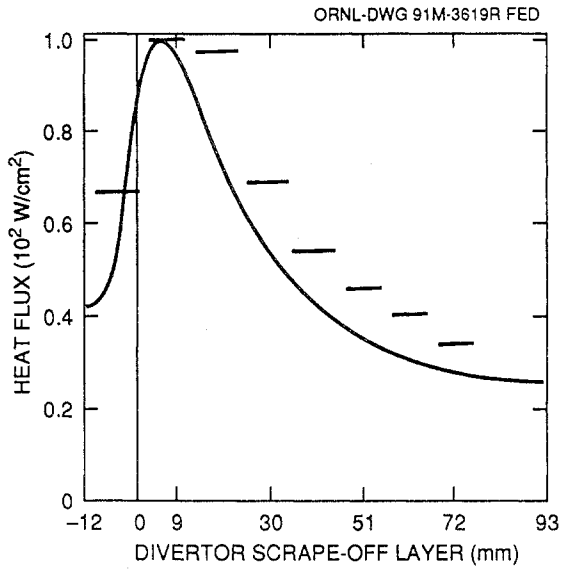


*FIG. 11. A B2 code fit of IRTV data at 4200 ms for the 7.5 MW, 1.25 MA case (shot 70903).*

TABLE II. INPUT AND OUTPUT VARIABLES IN THE B2 CODE

| Shot | $T_e^{sep,midpl}$ (eV) | $n_e^{sep,midpl}$ ($10^{13}$ cm$^{-3}$) | $T_{e,div}$ (eV) | $n_{e,div}$ ($10^{13}$ cm$^{-3}$) | $\Gamma_i$ ($10^{18}$ s$^{-1}$) | $Q_{div}$ (MW) | $Q_{sep}$ (MW) |
|---|---|---|---|---|---|---|---|
| | (a) | (a) | (b) | (b) | (b) | (c) | (d) |
| 70903, near the ring | 90 | 2.0 | 10.0 | 9.5 | 14.5 | 0.13 | 1.43 |
| 70903, away from the ring | 60 | 1.0 | 14.0 | 4.2 | 2.4 | 0.21 | 1.23 |
| 70902, near the ring | 220 | 3.0 | 2.2 | 28.0 | 27.0 | 0.28 | 3.80 |
| 70902, away from the ring | 85 | 1.6 | 2.0 | 7.5 | 11.8 | 0.14 | 2.80 |

**Note:** These data were chosen from a series of B2 runs on the basis that the $T_e^{sep,midpl}$, $n_e^{sep,midpl}$ and $Q_{div}$ values were closest to the measured values from Thomson scattering and the IRTV. The input variables are those in the first and second columns and the second and fourth members of the second last column.

(a) Value at mesh boundary (0.4 mm inside separatrix).

(b) Maximum value.

(c) Integral of the divertor target heat flux density over the B2 mesh.

(d) Total power across the separatrix.

When modelling the plasma when the ODI was under the bias ring, we assumed that the edge transport coefficients found above remained unchanged. However, as shown by the Thomson scattering data of Table I, with the ODI near the ring and at the time of peak baffle pressure, the midplane temperature and density at the separatrix were higher than the corresponding values with the ODI away from the bias ring. This may be due to additional recycling from the top of the bias ring and under the throat. Thus, in the B2 runs used with DEGAS to compute the peak baffle pressure, we changed the upstream boundary conditions to match these data and we added an additional recycling source at the face of the ring.

The recycling assumptions in the B2 code are as follows: for the 3900–4200 ms case, when the plasma is away from the bias ring, a distant wall is used (a conformal map geometry with distance from separatrix at divertor plate to wall of more than 20 cm), while for the case at about 3300 ms, when the ODI is near the ring, a narrow geometry (distance about 4 cm) is used. There is negligible recycling from the distant wall in the 3900 ms case. For the 3300 ms case, a recycling coefficient of 1 is taken at the boundary flux surface, for a height equal to the height of the ring above the tiled floor. It is assumed to be zero above that. Thus, there is an additional recycling of all the cross-field flux over the region corresponding to (mocked up as) the bias ring.

The recycling coefficients on the divertor plate and bias ring were assumed to be 0.99, as above. As a result of these changes, in the $P_{NBI}$ = 7.5 MW case, the particle flux to the targets increased by about a factor of 2.5 from that computed for the case of the ODI well away from the ring. In this case, the flux amplification factor rose from 9.3 to 20 because of the increased amount of recycling.

### 4.2.2. *Neutrals modelling results*

We used the edge plasma transport coefficients, as determined above, to generate the divertor plasma profiles with B2 and we input these profiles into DEGAS to calculate the peak pressure under the baffle. Figure 12 shows the resulting $n_e$, $T_e$ and particle flux profiles for $P_{NBI}$ = 7.5 MW. These profiles are from a single B2 run (i.e. the ODI is fixed) and the parameters are plotted versus radial position relative to the ODI (at the target plate). Using these fluxes as input, DEGAS neutrals modelling predicts a peak pressure of 5 mtorr, compared with the measured value of 7.7 mtorr for this case. The agreement is well

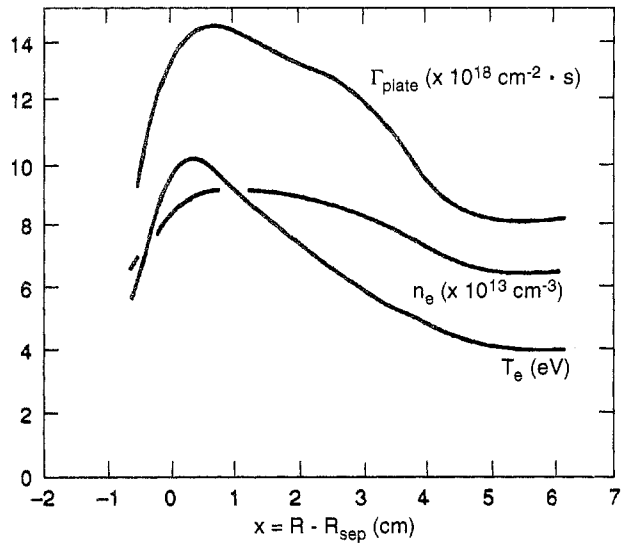


*FIG. 12. The $n_e$, $T_e$ and particle flux, $\Gamma_{plate}$, profiles that result from the B2 modelling and that are used as inputs to the DEGAS code for the 7.5 MW, 1.25 MA case (shot 70903).*

within the error bars resulting from uncertainties in the plasma profiles at the divertor target. In addition, the particle collection efficiencies computed by DEGAS are also of the order of 0.1, in agreement with our estimate in the introduction.

Next we examined the dependence of the pressure on the gap geometry at fixed injected power. We found this spatial dependence to be very sensitive to the details of the $T_e$ and $n_e$ profiles on the divertor floor, and we could not obtain good agreement with the experimental results. For example, to simulate the experimental points of Fig. 5(a), we had to use an electron density profile that is much steeper than the one obtained from the B2 code and shown in Fig. 12. If we used the profiles from B2, then we obtained a much weaker dependence on the gap, owing to the fact that with larger gaps there is less plasma to attenuate the neutrals before they enter the throat. Direct measurements of plasma parameters and profiles at the throat entrance are needed before a more detailed comparison can be attempted.

Perhaps more importantly, these DEGAS simulations neglected non-linear effects since the ring was not allowed to modify the profiles of $n_{e,div}$ and $T_{e,div}$ (either shape or amplitude) as the gap was varied. That is, the spatial dependence of the pressure was modelled by gradually extending the entrance of the throat (the bias ring) inward from large to small radius (i.e. towards the separatrix). Apart from truncating the outermost part of the SOL plasma, the presence of the ring did

not alter the divertor particle flux, plasma density or temperature. In reality, trapping neutrals under the baffle instead of letting them escape from the divertor region could increase the divertor flux and lower the plasma temperature as long as sufficient power is flowing in the SOL to maintain a nearly complete reionization. The study of such effects awaits a better simulation, which self-consistently couples the B2 plasma and DEGAS neutral codes. This work is now in progress.

Finally, we examined the scaling of peaked pressure with injected power. Here we found very good agreement with the experimental scaling. For example, in the $P_{inj} \simeq 14$ MW case, the higher $n_{e,sep}$, $T_{e,sep}$ from the Thomson scattering data led to higher amplification factors (of the order of 30–40 compared with of the order of 10 in the previous case) and lower temperatures ($< 2$ eV) in the B2 model. The scaling and peak values of divertor temperatures and densities from B2 agree with those of the Langmuir probes. With the B2 profiles at this power level, DEGAS is used to compute a neutral pressure of 13 ($\pm 7$) mtorr, as compared with the measured pressures of 10 to 13 mtorr. The error bar on the computed pressure is based on sensitivity studies in which the electron density and temperature from B2 are varied by up to a factor of two.

## 5. CONCLUSIONS

We have measured neutral particle pressures under the new divertor baffle of DIII-D that are sufficiently high to allow for particle control with the addition of a pump in that region. These pressures scale favourably with injected power and are sensitive to the separation between the ODI and the bias ring at the entrance of the baffle region. These experimental results were modelled successfully with a combination of a 2-D edge plasma code and a 3-D neutrals code (used here only in two dimensions owing to toroidal symmetry), in the sense that both the magnitude and, roughly, the scaling of the neutral pressure with injected power can be predicted. However, a higher level of detail in SOL measurements, especially in the divertor region near the bias ring, is required for successful modelling of the dependence of the neutral pressure on the separatrix to ring gap geometry.

## ACKNOWLEDGEMENTS

The authors thank T. Petrie for valuable advice in planning the experiments, T. Carlstrom for equally valuable advice on the use of the multipulse Thomson scattering data, and P.K. Mioduszewski and R.D. Stambaugh for their support and encouragement in this work.

In the analysis of the dependence of the pressure on magnetic geometry we consulted L.L. Lao, E.A. Lazarus and T.S. Taylor on the proper use of the magnetics code. The fast ionization gauges used, often referred to as ASDEX gauges, were developed by G. Haas of the ASDEX group (presently of ASDEX-Upgrade). His advice on the use of the gauges, as well as that of G.L. Jackson and T.E. Evans, who have in the past operated such gauges on DIII-D and on TEXT, made important contributions to this work. The technical support from R. Ellis of Lawrence Livermore National Laboratory and T.F. Rayburn of Oak Ridge National Laboratory in the construction and installation of the fast ion gauge assembly under the baffle is also acknowledged.

This work was supported by the United States Department of Energy under Contracts DE-AC05-84OR21400 with Martin Marietta Energy Systems, Inc., DE-AC03-89ER51114 with General Atomics, W-7405-ENG-48 with Lawrence Livermore National Laboratory and DE-AC03-76DP00789 with Sandia National Laboratories. One of the contributing authors (R.M.) was supported by a Magnetic Fusion Energy Technology Fellowship from the United States Department of Energy, administered by the Oak Ridge Associated Universities, and was advised by J.G. Gilligan at North Carolina State University.

## REFERENCES

[1] ANDERSON, P.M., BAXI, C.B., REIS, E.E., SCHAFFER, M.J., SMITH, J.P., Fusion Technology 1990 (Proc. 16th Symp. London, 1990), North-Holland, Amsterdam (1991) 336.

[2] HAAS, G., POSCHENRIEDER, W., NEUHAUSER, J., et al., J. Nucl. Mater. **162–164** (1989) 509.

[3] MAHDAVI, M.A., SCHAFFER, M., MIODUSZEWSKI, P., et al., The DIII-D Collaborative Advanced Divertor Program, Rep. GA-A19547, General Atomics, San Diego (February 1989).

[4] SCHAFFER, M.J., MAHDAVI, M.Ali, KLEPPER, C.C., HILL, D.N., RENSINK, M.E., Nucl. Fusion **32** (1992) 855.

[5] HEIFETZ, D.B., POST, D., PETRAVIC, M., WEISHEIT, J., BATEMAN, G., J. Comput. Phys. **46** (1982) 309.

[6] MIODUSZEWSKI, P.K., OWEN, L.W., MENON, M.M., HOGAN, J.T., J. Nucl. Mater. **176&177** (1990) 733.

[7] MAHDAVI, M.A., SCHAFFER, M.J., ANDERSON, P., et al., in Plasma Physics and Controlled Nuclear Fusion Research 1990 (Proc. 13th Int. Conf. Washington, DC, 1990), Vol. 1, IAEA, Vienna (1991) 335.

[8] HAAS, G., GERNHARDT, J., KEILHACKER, M., MESERVEY, E.B., ASDEX TEAM, J. Nucl. Mater. **121** (1984) 151.
[9] KLEPPER, C.C., EVANS, T.E., HAAS, G., JACKSON, G.L., MAINGI, R., J. Vac. Sci. Technol., A Vac. Surf. Films **11** (1993) 446.
[10] BUCHENAUER, D., HSU, W.L., SMITH, J.P., HILL, D.N., Rev. Sci. Instrum. **61** (1990) 2873.
[11] HILL, D.N., ELLIS, R., FERGUSON, W., et al., Rev. Sci. Instrum. **59** (1988) 1878.
[12] LAO, L.L., ST JOHN, H., STAMBAUGH, R.D., KELLMAN, A.G., PFEIFFER, W., Nucl. Fusion **25** (1985) 1611.
[13] LAO, L.L., FERRON, J.R., GROEBNER, R.J., et al., Nucl. Fusion **30** (1990) 1035.
[14] BUCHENAUER, D., J. Nucl. Mater. **176&177** (1990) 528.
[15] HARDTKE, A., FINKEN, K.H., REITER, D., et al., J. Nucl. Mater. **162–164** (1989) 661.
[16] POST, D.E., LANGER, W.D., PETRAVIC, M., J. Nucl. Mater. **121** (1984) 171.
[17] ALLEN, S.L., RENSINK, M., HILL, D.N., et al., J. Nucl. Mater. **162–164** (1989) 80.
[18] BRAAMS, B.J., A Multi-Fluid Code for Simulation of the Edge Plasma Turbulence in Tokamaks, NET Rep. EUR-FU/XII-80/87/68, Next European Torus Team (1987).
[19] RENSINK, M., HILL, D.N., MILOVICH, J., et al., Bull. Am. Phys. Soc. **35** (1990) 2024; HILL, D.N., RENSINK, M., FUTCH, A., et al., J. Nucl. Mater. **176&177** (1990) 158.

(Manuscript received 22 June 1992
Final manuscript received 9 November 1992)